

Accurate retrieval of ionization times by means of the phase-of-the-phase spectroscopy, and its limitsD. Würzler^{1,2,*}, S. Skruszewicz^{1,2,†}, A. M. Saylor,¹ D. Zille,¹ M. Möller,^{1,2}
P. Wustelt,^{1,2} Y. Zhang,^{1,2} J. Tiggesbäumker,³ and G. G. Paulus^{1,2}¹*Institute of Optics and Quantum Electronics, Friedrich Schiller University Jena, Max-Wien-Platz 1, 07743 Jena, Germany*²*Helmholtz Institute Jena, Fröbelstieg 3, 07743 Jena, Germany*³*Institute of Physics, University of Rostock, Albert-Einstein-Str. 23, 18059 Rostock, Germany*

(Received 22 November 2019; accepted 27 February 2020; published 31 March 2020)

By applying recently introduced, phase-of-the-phase spectroscopy [S. Skruszewicz *et al.*, *Phys. Rev. Lett.* **115**, 043001 (2015)], we analyze the phase-dependent photoelectron signal from Xe ionized in intense, parallel, two-color (1800 nm and 900 nm) laser fields. With such a field configuration, tuning of the relative phase between the ionizing, ω , and the perturbative, 2ω , field results in a modulation of the ionization rate, as well as modifications of the trajectories of electrons propagating in the laser-dressed continuum. Based on a semiclassical model, we confirm that phase dependencies, due to the perturbation of the ionization rate, encode the ionization times of the electrons. Here, using the fork structure, a well-known feature originating from well-defined dynamics allows us to distinguish between electrons ionized within distinct time windows. However, due to the simultaneous perturbation of the electron trajectories, the assignment of the ionization times can be distorted by up to 80 as, i.e., a 10° phase shift, which is independent of the degree of the perturbation.

DOI: [10.1103/PhysRevA.101.033416](https://doi.org/10.1103/PhysRevA.101.033416)**I. INTRODUCTION**

Sculpting the electric field of ultrashort laser pulses is a powerful tool to probe and control electron dynamics on their natural attosecond time scale. Introducing a controllable perturbation can selectively enhance a particular ionization channel and provides additional information on the underlying physical mechanisms. Specifically, this information is encoded in the phase-dependent yield of dissociation products [1,2], electrons [3–5], and high harmonic radiation [6–8]. To date, various schemes to shape the laser waveform have been demonstrated including controlling the carrier-envelope phase (CEP) [9] in few-cycle pulses, shaping of the polarization [10–12], or varying the pump-probe delay between two laser fields of different frequencies [13].

In recent years, experiments with two-color waveforms (ω , 2ω), generated by the coherent overlap of a strong fundamental field driving the dynamics with its weak second harmonic acting as a perturbation, have received considerable attention [4,14–16]. Analyzing the dependence of photoelectron momentum distribution (PMD) spectra as a function of the relative phase difference, φ_{rel} , between the ω and 2ω fields reveals unique fingerprints, which encode the dynamic response of the system. This method has been termed “phase-of-the-phase” spectroscopy [17] and allows one to capture these changes in just two parameters: (i) the relative phase contrast (*RPC*), which gives information about the strength of the photoelectron yield modulation, and (ii) the phase-of-the-phase (*PP*), which links the phase of the periodic photoelectron signal modulation to φ_{rel} [17–19].

The most important spectral features like the holographic sidelobes [20,21], the high-energy plateau [22,23], and the off-axis three-pronged fork structure [24] originate from scattering due to the laser-field assisted revisiting of the electron wave packets to the parent ion. Examples of these features can be seen in Fig. 1(a). The holographic sidelobes are visible as vertical stripes (label 1) and originate from the interference between the plain and the scattered spherical electron wave packets; the high-energy plateau (label 2) is created by backscattering of the revisiting electrons and the fork structure (label 3) results from scattering at different subsequent returns.

The strongly nonlinear dependence of the tunneling ionization process on the electric-field amplitude can be used to selectively enhance the electron trajectories with respect to their ionization time within the laser cycle, i.e., with subcycle resolution, by the perturbative 2ω field. This generates distinct phase dependencies in the electron spectrum, which can be traced back to the ionization times using phase-of-the-phase spectroscopy. This technique has been utilized to identify the electron trajectories ionized during consecutive half-cycles of the laser pulse [17,25–27]. Further, attosecond time resolution has been demonstrated by retrieving the ionization time delays from the Freeman resonances [28] and between electron trajectories forming holographic sidelobes [29].

However, the precise determination of the ionization time is significantly reduced due to the intrinsic effects the perturbation has on the propagation of the electronic wave packet in the laser-dressed continuum. Namely, modulations of vector potential and scattering times by the 2ω field introduce an additional weak functional dependence, which modulates the resulting photoelectron momentum spectrum. Quantitative discussion of this effect has remained elusive up to now.

In this paper, we report on a limit set on the precision of the retrieval of the ionization times in a phase-of-the-phase

*daniel.wuerzler@uni-jena.de

†slawomir.skruszewicz@uni-jena.de

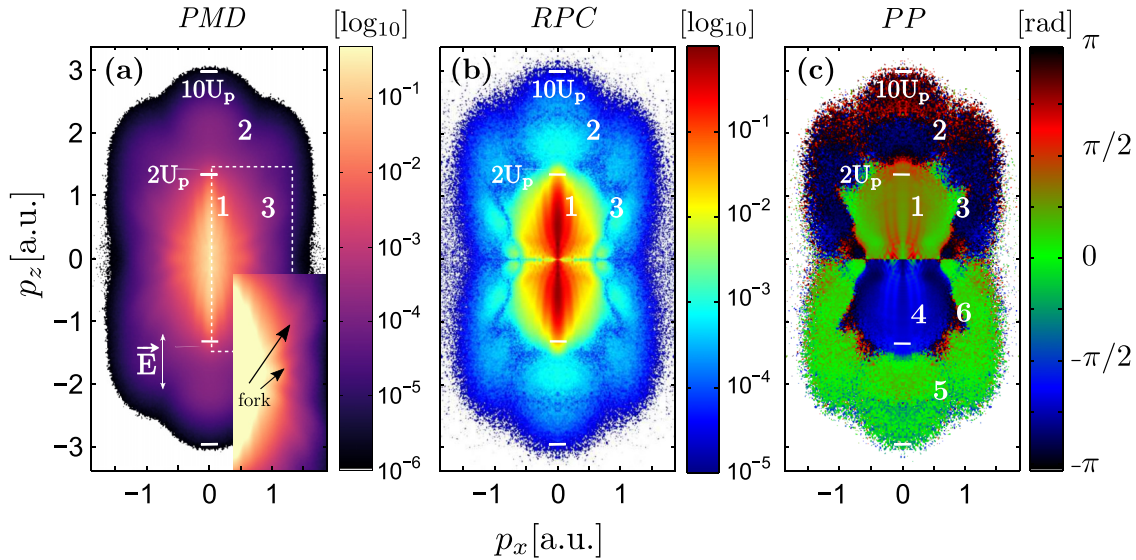


FIG. 1. Experimental results for laser-induced ionization of Xe atoms with intense ω , 2ω laser pulses (1800 nm, 900 nm) at intensities of $I_\omega = 4 \times 10^{13}$ W/cm² and $I_{2\omega} = 4 \times 10^{11}$ W/cm². (a) Photoelectron momentum distribution (PMD) resulting from the accumulation of phase-dependent measurements recorded for $\varphi_{\text{rel}} \in [0, 2\pi]$. The polarization axis is labeled with an arrow. The inset shows an enlarged section of the PMD (dashed rectangle) with enhanced contrast, focusing on the fork feature (see arrows). The relative phase contrast [RPC (b)] and the phase-of-the-phase spectra [PP (c)]. The RPC and PP spectra are extracted from the Fourier transformation of the φ_{rel} dependent photoelectron spectrum. See text for further details.

measurement due to perturbations of electron trajectories by the weak 2ω component. This is of broad ranging significance as retrieving time information from phase-dependent spectra has become a standard technique to reveal the underlying laser-driven electron dynamics. To facilitate this study and determine the precision of the ionization time retrieved from the phase-of-the-phase, one needs to use a region of the electron spectrum where a single process with well-defined ionization times dominates. This is not the case for the majority of the momentum-dependent electron spectrum, e.g., the plateau region where signals from multiple returns strongly overlap or processes with a broad range of ionization times contribute to narrow ranges of final momenta.

However, at 1800 nm wavelength, the photoelectron momentum distribution exhibit the so-called fork structure [24] with prongs corresponding to distinct rescattering processes and ionization times. Specifically, rescattering upon the electron's subsequent encounters with the parent ion lead to different prongs. Thus the phase dependencies, which are encoded by both the photoelectron yield and the laser-driven trajectories, can unambiguously be disentangled for the momentum intervals corresponding to these prongs. This allows us to determine that for weak 2ω perturbations the ratio of both contributing effects becomes independent of the degree of the perturbation. In other words, the modification of the ionization rate and the modification of the electron trajectories by the 2ω field are independent of the strength of the 2ω field. This can mislead assignment of the ionization times by up to 80 as.

II. EXPERIMENTAL SETUP

In the experiment, two-color laser waveforms with parallel polarizations (ω , 2ω) and adjustable relative phase, φ_{rel} , are generated in a collinear scheme [8]. Briefly, an optical

parametric amplification system (OPA, HE-TOPAS) is pumped by 40 fs pulses with pulse energies of up to 10 mJ from a Ti:sapphire laser system (1 kHz, 798 nm). The idler output tuned at 1800 nm ($\tau \approx 50$ fs, $E = 10.5$ mJ) is frequency doubled in a 250 μm BBO crystal (type I). A 92- μm -thick quartz wave plate acting as half-wave plate for 1800 nm (ω) and as full-wave plate for 900 nm (2ω) aligns the polarization of both fields in the same direction. We note that, at the given wavelength, the group-velocity mismatch is negligible (<4 fs) and its compensation by a birefringent crystal is not required.

The relative phase, φ_{rel} , of the ω , 2ω waveform is precisely controlled by a pair of motorized fused silica wedges in a range of $\varphi_{\text{rel}} \in [0, 2\pi]$. Their position is randomized during the experiment to account for laser intensity drifts and the data is subsequently sorted to retrieve the phase dependence. We remove any orthogonal polarization component by a broadband polarizer (CODIXX, $\sim 10^6$ contrast). The laser pulses are focused by a silver mirror ($f = 125$ mm) onto the atomic Xe beam generated by a pulsed valve operating at 1 kHz (Amsterdam Valve). The 3D photoelectron momentum distribution is projected onto a position sensitive detector (Chevron multichannel plate with P43 phosphorous screen) by a thick-lens velocity map imaging spectrometer (VMI) [26,30]. Gating of the multichannel plates is realized by using 150 ns pulses generated by a high voltage switch (Behlke GHTS60) in order to suppress spurious signals from secondary electrons and statistical noise.

III. RESULTS

The photoelectron momentum distribution resulting from the accumulation of individual phase-dependent measurements for $\varphi_{\text{rel}} \in [0, 2\pi]$ is shown in Fig. 1(a). Beside the

spectral features described in the introduction, i.e., holographic sidelobes (label 1), high-energy plateau (2), and the fork structure (3), the cutoff energies $10U_p$ and $2U_p$ [ponderomotive energy $U_p = I/(4\omega^2)$] of scattered and unscattered electron are indicated. The 2ω field introduces perturbations to the strong-field ionization process and generates pronounced modulations on the photoelectron yields varying predominantly with the 2ω field periodicity. In order to quantify these changes, we Fourier analyze the photoelectron yield with respect to φ_{rel} for each final momentum $\mathbf{p} = (p_x, p_z)$. By considering only the first-order term,

$$Y(\mathbf{p}, \varphi_{\text{rel}}) \simeq RPC(\mathbf{p}) \cdot \cos[\varphi_{\text{rel}} + PP(\mathbf{p})] + c, \quad (1)$$

the relative-phase contrast, $RPC(\mathbf{p})$, and phase-of-the-phase, $PP(\mathbf{p})$, spectra are extracted; see Figs. 1(b) and 1(c), respectively.

Broadly speaking, the PP spectrum, see Fig. 1(c), essentially consists of four regions. Regions labeled (1) and (5) with $PP \sim 0$ (red to green in figure) and regions labeled (2) and (4) with $PP \sim \pm\pi$ (blue to black in figure). This π shift corresponds to the emission during two consecutive laser half-cycles [17]. In order to identify the aforementioned fork structure, which is chosen for its well-defined ionization times that allow for determination of the trajectory perturbation effects, we use the PMD and PP spectra, where the fork pattern is visible; see Figs. 1(a) and 1(c), region 3.

IV. MODELING

To trace the dynamics backwards from the momentum-dependent electron spectrum to the corresponding ionization time, the evolution of the system in the ω , 2ω field is modeled analytically in terms of the semiclassical model (SCM) as comprehensively discussed in [26]. This allows one to divide the interaction of an atomic system with a strong laser field into two steps: (i) tunneling and (ii) propagation of classical trajectories in the laser-dressed continuum. The two-color vector potential described in dipole approximation,

$$\mathbf{A}(t, \varphi_{\text{rel}}) = A_0 \mathbf{e}_z [\sin(\omega t_i) + 0.5\xi \times \sin(2\omega t + \varphi_{\text{rel}})], \quad (2)$$

enables the investigation of the impact of the perturbative 2ω field on the phase-dependent electron yield. Here, φ_{rel} is the relative phase, \mathbf{e}_z is a unit vector defining the polarization direction, and $\xi = E_{2\omega}/E_\omega$ defines the ratio between the electric-field amplitude of the ω and 2ω components. To ensure that the dynamics are independent of the field's envelope and depend only on φ_{rel} , flat-top laser pulses are used.

The instantaneous tunneling rate is modeled by the ADK rate [31]: $W_i(t_i) \sim \exp\{-2/[3|\mathbf{E}(t_i)|]\}$. The ionization time, t_i , determines the initial conditions for classical equation of motion of the electron in the electric field of the laser pulse, $\mathbf{E}(t) = -\frac{\partial}{\partial t}\mathbf{A}(t)$. Revisiting the parent ion, the electronic wave packet rescatters at time, t_r , with momentum, $\mathbf{p}_{\text{ret}} = \mathbf{A}(t_r) - \mathbf{A}(t_i)$. The weight of each classical trajectory is proportional to $W_{\text{total}} = W_i(t_i)W_r(\mathbf{p}_{\text{ret}})W_{DCS}(\mathbf{p}_{\text{ret}})$. Here, W_r is the scattering probability and W_{DCS} is the elastic differential scattering cross section (DCS) which takes the angular photoelectron distribution into account. W_{DCS} is calculated numerically in the single-active-electron approximation for the xenon model potential described in [32,33]. W_r is calculated

by finding the intersection of the returning wave packet with the total cross section, σ , derived from W_{DCS} [26].

Here we consider three cases: (ϵ_{ion}) only the perturbations of the tunneling probability are taken into account, (ϵ_{trj}) only the perturbation of the propagation of classical trajectories due to the 2ω field are taken into account, and (ϵ_{tot}) both effects are taken into account. The assumptions ϵ_{ion} and ϵ_{trj} generate two distinct functional phase dependencies in the form of Eq. (1), with phases PP_{ion} and PP_{trj} , respectively. In case ϵ_{ion} the phase-dependent tunneling probability modulates the electron yield generated at the ionization time, t_i . As mentioned before, the tunneling rate exponentially depends on the absolute electric field at time of ionization, t_i . Thus, for weak perturbations, it depends on the relative phase as $\pm \cos(2\omega t_i + \varphi_{\text{rel}}) + c$ and maximizes when $\varphi_{\text{rel}}^{\text{max}} = -2\omega t_i$ or $\varphi_{\text{rel}}^{\text{max}} = \pi - 2\omega t_i$. The two cases correspond to ionization times within odd or even half-cycles of the ω field. According to the relation $PP_{\text{ion}} = -\varphi_{\text{rel}}^{\text{max}}$, the information on the ionization time is encoded in the PP_{ion} value by

$$PP_{\text{ion}} = 2\omega t_i \quad \text{or} \quad PP_{\text{ion}} = 2\omega t_i - \pi. \quad (3)$$

It is essential to note that for each final momentum, (p_x, p_z) , the signals from multiple classical trajectories overlap. Thus $PP_{\text{ion}}(p_x, p_z)$ encodes the average ionization time of all contributing trajectories weighted by W_{total} .

In addition, the φ_{rel} -dependent vector potential [Eq. (2)] modulates the return time, t_r , of the electron's trajectory and, therefore, also both the return momentum $\mathbf{p}_{\text{ret}}(t_r)$ and the vector potential $\mathbf{A}(t_r)$. The resulting yield modulations in the electron spectrum are periodic with respect to the 2ω field and generate an additional functional dependency with phase PP_{trj} . The corresponding phase, PP_{trj} , turns out to be a rather complex function of the ionization and rescattering times, which prevents a straightforward interpretation. Nevertheless, the effective electron yield modulations, resulting from both of the aforementioned φ_{rel} dependencies, can be expressed as a sum of two cos-like functions with phases PP_{ion} and PP_{trj} . Their weights stem from their amplitudes encoded in RPC . Applying the harmonic addition theorem results in a new phase dependence, PP_{total} , encoding information on the ionization time, PP_{ion} , convoluted with the trajectory perturbation, PP_{trj} . Due to the exponential scaling of the tunneling probability with $|\mathbf{E}(t_i)|$, we expect the corresponding PP_{ion} term to dominate the total phase, PP_{total} , for large ξ . However, PP_{trj} also contributes and may be significant for small ξ .

In order to quantify the significance of PP_{trj} , we compare the aforementioned scenarios, i.e., ϵ_{ion} , ϵ_{trj} , and ϵ_{tot} . Namely, we compare PP dependencies generated by each model in the fork structure, where the ionization times are well confined. The PP signals are extracted by Fourier transformation of the phase dependent SCM spectra calculated for $\varphi_{\text{rel}} \in [0, 2\pi]$. To match the measurement conditions, we calculate the Abel projections of the 3D SCM spectra onto the p_x - p_z plane.

V. DISCUSSION

The experimental PP spectrum and the results of the numerical calculations for model ϵ_{tot} (which includes the perturbation effect on the tunneling probability and on the

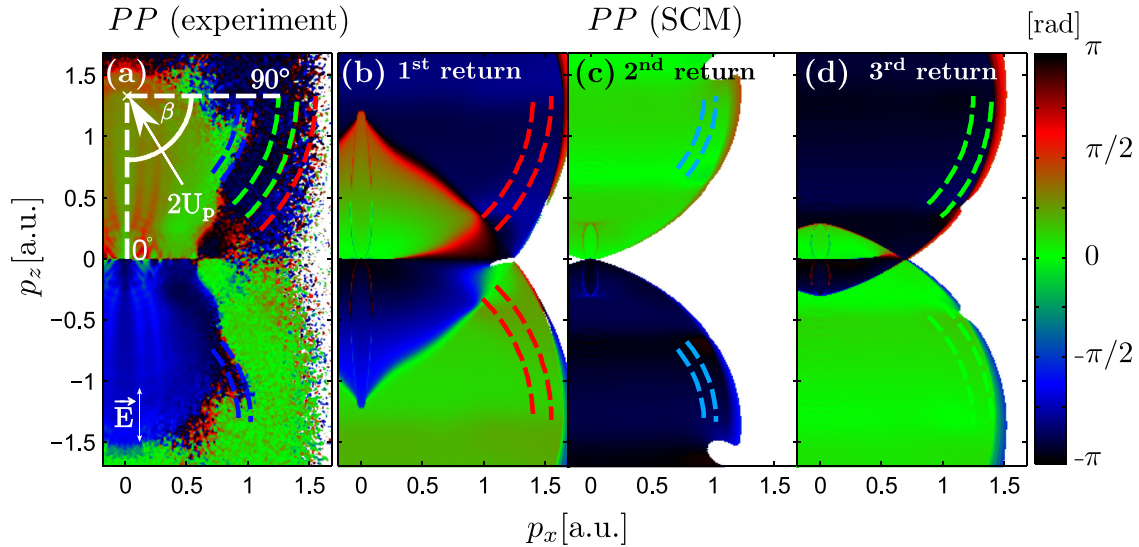


FIG. 2. Comparison of the measured and simulated PP spectra. (a) The experimental spectrum, identical to Fig. 1(c). (b)–(d) The SCM- PP spectra are obtained from numerical calculations for each individual return. Signals from later returns can be extracted from the fork structure; see dashed lines (red: first; blue: second; green: third return). The angle β (see left panel) parametrizes the angular coordinate.

trajectories for each return) are shown in Fig. 2. Essentially, the trajectories rescattering at the first return, Fig. 2(b), reproduce the majority of the PP dependencies in the experimental spectrum. This is due to the electron wave packet dispersion, which significantly reduces the rescattering probability for higher-order returns [34]. The angular distributions introduced by W_{DCS} lead to the appearance of horizontal stripes [e.g., in the green area of Figs. 2(b) and 2(d)], which weakly modulate the PP signal.

We enclose the regions of enhanced rescattering signals in the fork structure by the arcs of the rings centered at $2U_p$, where U_p is the ponderomotive energy. The electrons in this area originate from a specific return. Further, the electrons at different angles along this arc have different scattering angles, ionization times, ionization probabilities, and trajectories. Therefore, to allow for a more in depth analysis of the perturbations, it is convenient to introduce an angle, β , to parametrize the angular coordinate. Namely, in order to extract the PP signals we integrate the electron spectra along the radial coordinate over 5° bins for $\beta \in [40^\circ, 80^\circ]$ and Fourier transform the results.

To illustrate the importance of the inclusion of the trajectory perturbation due to the 2ω field, the essential findings of our analysis are summarized in Fig. 3, where we plot the PP dependencies extracted from the fork regions as a function of the angular coordinate β . The three panels show results for (a) the first, (b) the second, and (c) the third returns. The experimental data (squares) have error bars showing the uncertainty of the PP determination resulting from a cosine fit of the integrated photoelectron yield within the region of interest. The results of the numerical calculations for $\xi = 0.01$ are plotted with lines. Here one sees that the model including only the ionization perturbation (ϵ_{ion} , blue dashed line) comes close to reproducing the experimental results. However, the inclusion of the perturbation of the trajectories (ϵ_{tot} , black solid line) significantly modifies the PP and more closely fits the experimental data. Moreover, to illustrate the importance

of the trajectory perturbation, the PP is plotted using the ionization perturbation $\xi_{ion} = 0.01$ and the trajectory perturbation $\xi_{trj} = 0.005$ (ϵ'_{tot} , yellow dotted line) to illustrate the effect of a weaker trajectory perturbation. For comparison, the PP behavior including only perturbation of the trajectories (ϵ_{trj} , green dash-dotted line) is also shown in the inset for clarity.

To quantify the importance of including ϵ_{trj} , the calculated and measured $PP(\beta)$ data are compared. The SCM results for the first, Fig. 3(a), and the third, Fig. 3(c), return closely reproduce the angular dependencies, $PP(\beta)$, which result from numerically calculated W_{DCS} . The standard deviation between the experimental data of the first and third return with respect to the model ϵ_{ion} is $\sigma \simeq 10^\circ \simeq 80$ as, while inclusion of the trajectory perturbation reduces the value to $\sigma \simeq 3.6^\circ \simeq 30$ as. The larger discrepancies for the second return, Fig. 3(b), are due to an unfavorable overlap of the second return fork feature with the signal from the direct and rescattered electrons in this particular spectral region.

Moreover, using the SCM data, one can determine the validity of using the phase PP_{ion} to retrieve an ionization time without considering the perturbation to the trajectory. Neglecting the trajectory perturbation, PP_{ion} can directly be mapped on the average ionization time, \bar{t}_i , with Eq. (3), $\overline{PP}_{ion} = 2\omega\bar{t}_i - \pi$. For verification, we backtrace the trajectories forming the fork structure in the absence of the 2ω field and calculate the averaged ionization time, which are in excellent agreement with the ϵ_{ion} results.

This simplified retrieval procedure, which neglects the influence of the trajectory perturbation, can also be applied to the experimental data. Namely, the experimental results show that the trajectories rescattering at the second, Fig. 3(b), and third, Fig. 3(c), returns are ionized ~ 100 as closer to the peak of the electric field, $\bar{t} = 0$ as, than trajectories rescattering at the first return, Fig. 3(a). This is in rough agreement with the Simple Man's theory. Note, however, that this retrieval does not account for the trajectory perturbation. Thus the measured

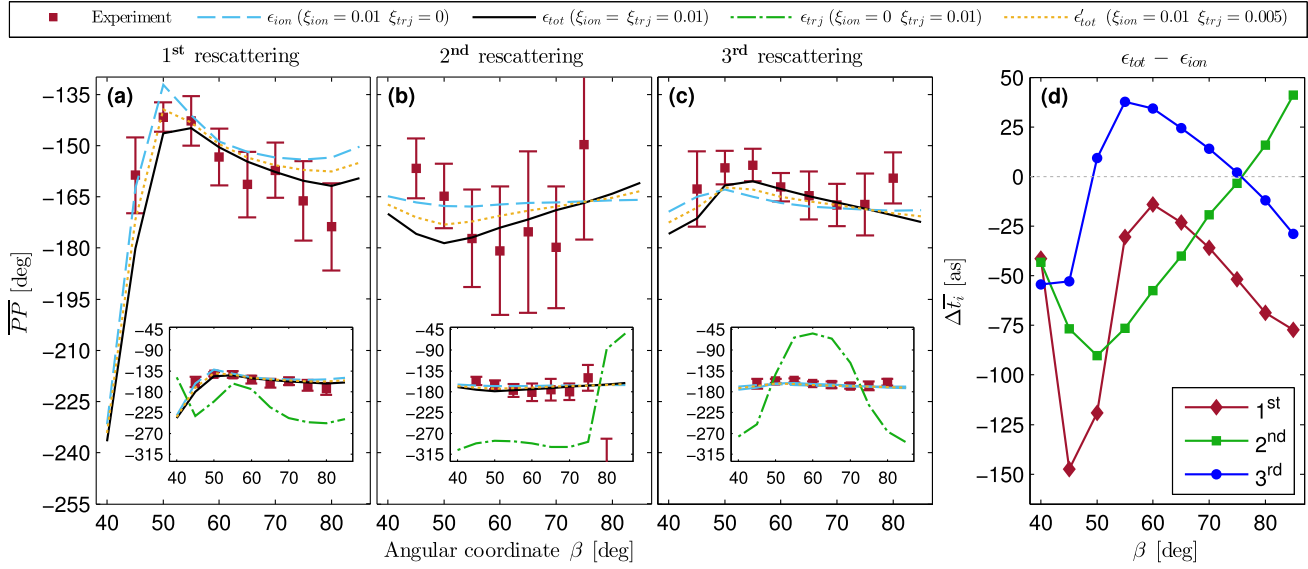


FIG. 3. \overline{PP} values extracted from fork region for first (a), second (b), and third (c) return shown in Fig. 2. Squares: experimental data points are integrated over 5° . Lines: results of SCM simulation for weak 2ω perturbation ($\xi = 0.01$) acting on the tunneling rate and the trajectories (ϵ_{tot} , black solid), only the tunneling (ϵ_{ion} , blue dashed), and only on the trajectories (ϵ_{trj} , green dash-dotted). The insets show significant deviation of experimental results from model ϵ_{trj} . A reduction of the perturbation of the trajectories in model ϵ_{tot} by a factor of two (i.e., $\xi_{ion} = 0.01$ and $\xi_{trj} = 0.005$) results in the yellow dotted lines (ϵ'_{tot}). Using $\bar{t}_i = (\overline{PP} + \pi)/(2\omega)$ to retrieve the ionization time \bar{t}_i , panel (d) shows the time offset $\Delta \bar{t}_i$ between ϵ_{tot} and ϵ_{ion} .

values are likely shifted as predicted by the offset $\Delta \bar{t}_i$ between the ϵ_{tot} and ϵ_{ion} data, Fig. 3(d). Most values of the absolute offset $|\Delta \bar{t}_i|$ vary between 0 as and 80 as with a mean value of 45 as.

In the quest to reduce this effect and enable a more precise conversion from the phase-of-the-phase, PP , to the ionization time, t_i , reduction of the perturbation, ξ , seem to be an obvious choice. However, numerical analysis supported by the experimental observation shows that, even for very low perturbative 2ω fields, $\xi \ll 1\%$, the functional dependencies resulting from the trajectories' perturbations cannot be neglected and add uncertainty to the retrieval of the ionization time encoded in the PP spectra.

In order to quantify the significance of this effect as a function of the perturbation, ξ , we calculate the relative-phase contrast averaged over the entire electron spectrum, $\overline{RPC}(\xi)$, for both the ionization perturbation, ϵ_{ion} , and the trajectory perturbation, ϵ_{trj} , shown in Fig. 4. As the weighted sum of these two terms determines the PP_{total} via the harmonic addition theorem, the ratio of these two terms $R = \overline{RPC}_{trj}/\overline{RPC}_{ion}$ quantifies the importance of the trajectory perturbation. Here we find that \overline{RPC}_{ion} increases exponentially with ξ as expected from the exponential scaling of the ionization probability with electric field. For small perturbations, $\xi < 0.05$, the function is well fit by the linear term of the Taylor series, the slope of which we label s_{ion} . Further, \overline{RPC}_{trj} scales linearly with ξ , resulting in a slope of s_{trj} . Thus, for vanishingly small perturbations, the ratio of the relative phase contrasts remains constant, $R(\xi < 0.05) = s_{trj}/s_{ion} = 0.17$, independent on the perturbation, ξ . Given this ratio, the largest phase shift from the model, which includes only the ionization perturbation, ϵ_{ion} , to the model, which includes both the ionization and the trajectory perturbation, ϵ_{tot} , occurs for an offset of

$|\overline{PP}_{ion} - \overline{PP}_{trj}| = 100^\circ$. Under these worst case conditions, the precise assignment of the ionization time can be misled by about 80 as (10°).

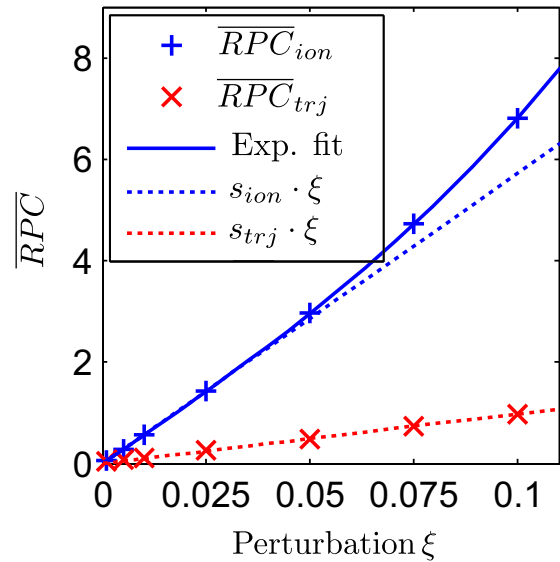


FIG. 4. Averaged RPC signal calculated numerically including perturbations to the tunneling probability (ϵ_{ion} , blue) and the trajectories in the laser-dressed continuum (ϵ_{trj} , red) as a function of perturbation (ξ). The RPC signal, which is due to the tunneling rate modification, follows an exponential growth (blue solid line) and can be approximated with a linear function for $\xi < 0.05$ (blue dotted line). The trajectories RPC signal scales linearly with ξ (red dotted line). In the weak perturbation regime, the ratio between both signals is constant (0.17), indicating that the trajectories contribution cannot be neglected.

As reducing the perturbation to a vanishingly small value does not remove the effects on the trajectory and $\overline{RPC}_{\text{ion}}$ increases exponentially, it may be tempting to move to large perturbations to facilitate the retrieval of the ionization time from the *PP*. However, for large perturbations, $\xi > 0.2$, the electric field of 2ω field is strong enough to start driving ionization. Further, the functional relation between the ionization and rescattering times loses its validity. For example, it is well known that, in the case of a strong second harmonic, there is a caustic effect where many trajectories ionized at different times, t_i , coalesce at the same rescattering time, t_r [35]. Thus, to allow for the most accurate retrieval of the ionization time from the *PP*, measurements should be performed at perturbation levels between $0.05 < \xi < 0.15$, to keep the trajectory dependent offset as small as possible.

VI. SUMMARY

In summary, we investigated the impact of perturbations of two-color, $\omega, 2\omega$, fields on the precise determination of the ionization time of rescattered electrons. We show that, in

addition to modifying the ionization rate, changing the relative two-color phase, φ_{rel} , changes the electron trajectories and final momenta. This generates a shift in the phase dependence of the photoelectron yield. Based on measurements and a simple semiclassical trajectory-based model, we deconvoluted the perturbative effects on ionization and the electron propagation and showed that the trajectory effects cannot be neglected even for extremely small perturbation fields, $\xi \ll 1\%$. In the fork region, we find that this effect can mislead the precise assignment of the ionization time by $t_i \simeq 80$ as $\simeq 10^\circ$. Our findings are of broad ranging significance as retrieving time information from phase-dependent spectra has become a standard technique. We identified a significant uncertainty in the direct retrieval of the average ionization time from the phase dependence, $\overline{PP}_{\text{ion}} = 2\omega\bar{t}_i$ or $\overline{PP}_{\text{ion}} = 2\omega\bar{t}_i - \pi$, due to perturbations of the electron trajectories.

ACKNOWLEDGMENTS

The authors acknowledge funding from Grant No. PA 730/7 (Priority Program 1840) and Grant No. TI 210-7/1 (SFB 652) of the Deutsche Forschungsgemeinschaft (DFG).

-
- [1] D. Ray, F. He, S. De, W. Cao, H. Mashiko, P. Ranitovic, K. P. Singh, I. Znakovskaya, U. Thumm, G. G. Paulus, M. F. Kling, I. V. Litvinyuk, and C. L. Cocke, *Phys. Rev. Lett.* **103**, 223201 (2009).
- [2] X. Xie, S. Roither, S. Larimian, S. Erattupuzha, L. Zhang, D. Kartashov, F. He, A. Baltuška, and M. Kitzler, *Phys. Rev. A* **99**, 043409 (2019).
- [3] D. Ray, Z. Chen, S. De, W. Cao, I. V. Litvinyuk, A. T. Le, C. D. Lin, M. F. Kling, and C. L. Cocke, *Phys. Rev. A* **83**, 013410 (2011).
- [4] X. Xie, S. Roither, D. Kartashov, E. Persson, D. G. Arbo, L. Zhang, S. Gräfe, M. S. Schöffler, J. Burgdörfer, A. Baltuška, and M. Kitzler, *Phys. Rev. Lett.* **108**, 193004 (2012).
- [5] J. Passig, S. Zherebtsov, R. Irsig, M. Arbeiter, C. Peltz, S. Göde, S. Skruszewicz, K.-H. Meiwes-Broer, J. Tiggesbäumker, M. F. Kling, and T. Fennel, *Nat. Commun.* **9**, 629 (2018).
- [6] C. Figueira de Morisson Faria, D. B. Milošević, and G. G. Paulus, *Phys. Rev. A* **61**, 063415 (2000).
- [7] D. Oron, Y. Silberberg, N. Dudovich, and D. M. Villeneuve, *Phys. Rev. A* **72**, 063816 (2005).
- [8] N. Dudovich, O. Smirnova, J. Levesque, Y. Mairesse, M. Y. Ivanov, D. M. Villeneuve, and P. B. Corkum, *Nat. Phys.* **2**, 781 (2006).
- [9] G. G. Paulus, F. Lindner, H. Walther, A. Baltuška, E. Goulielmakis, M. Lezius, and F. Krausz, *Phys. Rev. Lett.* **91**, 253004 (2003).
- [10] T. Brixner and G. Gerber, *Opt. Lett.* **26**, 557 (2001).
- [11] T. Brixner, G. Krampert, T. Pfeifer, R. Selle, G. Gerber, M. Wollenhaupt, O. Graefe, C. Horn, D. Liese, and T. Baumert, *Phys. Rev. Lett.* **92**, 208301 (2004).
- [12] I. J. Sola, E. Mevel, L. Elouga, E. Constant, V. Strelkov, L. Poletto, P. Villoresi, E. Benedetti, J.-P. Caumes, S. Stagira, C. Vozzi, G. Sansone, and M. Nisoli, *Nat. Phys.* **2**, 319 (2006).
- [13] M. Shapiro, J. W. Hepburn, and P. Brumer, *Chem. Phys. Lett.* **149**, 451 (1988).
- [14] D. Shafir, H. Soifer, B. D. Bruner, M. Dagan, Y. Mairesse, S. Patchkovskii, M. Y. Ivanov, O. Smirnova, and N. Dudovich, *Nature (London)* **485**, 343 (2012).
- [15] M. Förster, T. Paschen, M. Krüger, C. Lemell, G. Wachter, F. Libisch, T. Madlener, J. Burgdörfer, and P. Hommelhoff, *Phys. Rev. Lett.* **117**, 217601 (2016).
- [16] M. Richter, M. Kunitski, M. Schöffler, T. Jahnke, L. P. H. Schmidt, and R. Dörner, *Phys. Rev. A* **94**, 033416 (2016).
- [17] S. Skruszewicz, J. Tiggesbäumker, K.-H. Meiwes-Broer, M. Arbeiter, T. Fennel, and D. Bauer, *Phys. Rev. Lett.* **115**, 043001 (2015).
- [18] M. A. Almajid, M. Zabel, S. Skruszewicz, J. Tiggesbäumker, and D. Bauer, *J. Phys. B* **50**, 194001 (2017).
- [19] V. A. Tulsy, M. A. Almajid, and D. Bauer, *Phys. Rev. A* **98**, 053433 (2018).
- [20] Y. Huismans, A. Rouzée, A. Gijsbertsen, J. H. Jungmann, A. S. Smolkowska, P. S. W. M. Logman, F. Lépine, C. Cauchy, S. Zamith, T. Marchenko, J. M. Bakker, G. Berden, B. Redlich, A. F. G. van der Meer, H. G. Muller, W. Vermin, K. J. Schafer, M. Spanner, M. Y. Ivanov, O. Smirnova, D. Bauer, S. V. Popruzhenko, and M. J. J. Vrakking, *Science* **331**, 61 (2011).
- [21] M. Spanner, S. O. P. B. Corkum, and M. Y. Ivanov, *J. Phys. B* **37**, L243 (2004).
- [22] G. G. Paulus, W. Nicklich, H. Xu, P. Lambropoulos, and H. Walther, *Phys. Rev. Lett.* **72**, 2851 (1994).
- [23] Z. Chen, A.-T. Le, T. Morishita, and C. D. Lin, *Phys. Rev. A* **79**, 033409 (2009).
- [24] M. Möller, F. Meyer, A. M. Sayler, G. G. Paulus, M. F. Kling, B. E. Schmidt, W. Becker, and D. B. Milošević, *Phys. Rev. A* **90**, 023412 (2014).
- [25] J. Henkel and M. Lein, *Phys. Rev. A* **92**, 013422 (2015).

- [26] D. Würzler, N. Eicke, M. Möller, D. Seipt, A. M. Sayler, S. Fritzsche, M. Lein, and G. G. Paulus, *J. Phys. B* **51**, 015001 (2018).
- [27] J. Tan, Y. Li, Y. Zhou, M. He, Y. Chen, M. Li, and P. Lu, *Opt. Quantum Electron.* **50**, 57 (2018).
- [28] X. Gong, C. Lin, F. He, Q. Song, K. Lin, Q. Ji, W. Zhang, J. Ma, P. Lu, Y. Liu, H. Zeng, W. Yang, and J. Wu, *Phys. Rev. Lett.* **118**, 143203 (2017).
- [29] G. Porat, G. Alon, S. Rozen, O. Pedatzur, M. Kruger, D. Azoury, A. Natan, G. Orenstein, B. D. Bruner, M. J. J. Vrakking, and N. Dudovich, *Nat. Commun.* **9**, 2805 (2018).
- [30] N. G. Kling, D. Paul, A. Gura, G. Laurent, S. De, H. Li, Z. Wang, B. Ahn, C. H. Kim, T. K. Kim, I. V. Litvinyuk, C. L. Cocke, I. Ben-Itzhak, D. Kim, and M. F. Kling, *J. Instrum.* **9**, P05005 (2014).
- [31] M. V. Ammosov, N. B. Delone, and V. P. Krainov, *Zh. Eksp. Teor. Fiz.* **91**, 2008 (1986) [*Sov. Phys. JETP* **64**, 1191 (1986)].
- [32] M. Okunishi, T. Morishita, G. Prümper, K. Shimada, C. D. Lin, S. Watanabe, and K. Ueda, *Phys. Rev. Lett.* **100**, 143001 (2008).
- [33] X. M. Tong and C. D. Lin, *J. Phys. B* **38**, 2593 (2005).
- [34] D. B. Milosevic, G. G. Paulus, D. Bauer, and W. Becker, *J. Phys. B* **39**, R203 (2006).
- [35] D. Faccialà, S. Pabst, B. D. Bruner, A. G. Ciriolo, S. De Silvestri, M. Devetta, M. Negro, H. Soifer, S. Stagira, N. Dudovich, and C. Vozzi, *Phys. Rev. Lett.* **117**, 093902 (2016).